Controlled Patterning of Carbon Nanotube Energy Levels by Covalent DNA Functionalization

*Yu Zheng[1], Sergei M. Bachilo[1], and R. Bruce Weisman[1,2]**

[1] Department of Chemistry and the Smalley-Curl Institute, Rice University, Houston, TX 77005 USA

[2] Department of Materials Science and NanoEngineering, Rice University, Houston, TX 77005 USA

email address: weisman@rice.edu.

ABSTRACT

Each structural form of single-wall carbon nanotube (SWCNT) has specific electronic and optical properties, but it has not been possible to achieve spatial or energetic modulation of those properties in controllable ways. We present here a simple method for using chemical reactions with single-stranded DNA (ssDNA) to accomplish such modulation. When aqueous suspensions of SWCNTs coated with ssDNA are exposed to singlet oxygen under ambient conditions, the nanotubes selectively form covalent bonds to the guanine nucleotides. This locally modulates semiconducting SWCNT energy levels and red-shifts their emission wavelengths by up to 10%. Both the magnitude and spatial pattern of these shifts can be controlled by selecting the nucleotide sequence used to coat the nanotubes. Biomedical, opto-electronic, and single-photon emission applications are foreseen.

KEYWORDS: SWCNT, guanine nucleotides, singlet oxygen, exciton localization, band gap engineering

The unusual electronic and optical properties of single-wall carbon nanotubes (SWCNTs) have attracted intense attention from basic and applied researchers. SWCNTs exist in a variety of distinct structures, each indexed by a pair of integers, (*n*,*m*), and having a well-defined diameter, roll-up (chiral) angle, long-range crystalline order, and uniform electronic properties along its length.[1] Sparse chemical functionalization at random positions on the sidewalls of semiconducting SWCNTs has been shown to introduce local band gap changes that can trap mobile excitons and cause spectrally shifted luminescence.[2-7] Such chemically altered SWCNTs hold promise as single-photon emitters for quantum cryptography.[8-10] To date, however, it has not been possible to control the spatial pattern of covalent functionalization or to smoothly adjust the band gap modulation. We report here a simple method to achieve tailored sidewall functionalization of SWCNTs that can modulate electronic energy levels along the nanotube axis with customized spatial patterns and depths.

RESULTS AND DISCUSSION

The modulation is achieved by inducing a covalent reaction between the nanotube sidewall and guanine nucleotides in single-stranded DNA (ssDNA) oligos that wrap the nanotube. This reaction proceeds spontaneously and rapidly at room temperature in the presence of singlet ($^1\Delta_g$) oxygen, which is readily generated *in situ* by optically irradiating a sensitizer such as rose bengal. Each reacted guanine creates a local perturbation to the nanotube π-electron system, resulting in a red-shift of the characteristic band gap photoluminescence. Reactions with ssDNA oligo coatings that are rich in guanines give larger nanotube perturbations and greater spectral shifts. One can also coat the nanotubes with oligos containing segments that have different guanine contents to generate customized spatial patterns of π-electron energy shifts.

To induce the covalent functionalization reaction, we begin with an aqueous dispersion of SWCNTs in ssDNA,[11-12] and add a small concentration of rose bengal, a common dye. Irradiating the sample with light near the 550 nm rose bengal absorption peak efficiently generates the dye's triplet state through intersystem crossing.[13] This state is quickly quenched by energy transfer to dissolved O_2, forming the reactive $^1\Delta_g$ excited state commonly symbolized as $^1O_2$. It is known that $^1O_2$ reacts with guanine at a rate approximately two orders of magnitude greater than with other nucleobases.[14-17] The product is a guanine endoperoxide that likely undergoes rapid O-O bond cleavage followed by radical addition to an adjacent carbon atom of the SWCNT sidewall.

Irradiating an aqueous sample of CoMoCAT SWCNTs dispersed in $(GT)_{20}$ ssDNA oligos in the presence of rose bengal caused dramatic changes in the nanotube emission spectrum (see Figure 1A,B). Emission profiles taken at the (6,5) excitation maxima and plotted in Figure 1C reveal a red-shift in peak wavelength of 6.3%, spectral broadening by a factor of ~3, and an increase in integrated emission intensity to ~2.5 times that of the pristine sample. The absorption features became broadened and red-shifted (see Figure 1E and S1).Two observations strongly indicate that the treated nanotubes have been covalently functionalized. First, the Raman D/G band intensity ratio increased on treatment from 0.08 to 0.36, implying greater electronic scattering caused by conversion of SWCNT carbon atoms from sp^2 to sp^3-hybridization.[18] As shown in Figures. S2, S3, and Table S1, we also found that the altered emission persisted after immersing the treated nanotubes in a 0.5% solution of sodium deoxycholate, a strong surfactant that is known to displace noncovalent coatings of ssDNA on SWCNTs.[19]

To investigate the nature of spectral broadening in the shifted (E_{11}*) band, we used short-wave infrared fluorescence microscopy to measure spectra of individual SWCNTs in a treated

sample heavily diluted with sodium deoxycholate. A typical single-particle E_{11}^* emission spectrum is plotted in Figure 1D. These spectra show full-widths at half-maximum that are ca. 65 to 80% that of the bulk sample (see Figure S6A and Table S2). This indicates that there is a substantial distribution of peak wavelengths within the treated bulk sample. The observed width is also several times greater than that of an individual pristine (6,5) SWCNT, suggesting spectral inhomogeneity within a single treated nanotube. To confirm that the E_{11}^* emission in fact arises from nanotube excitons rather than from localized addend states, we measured its excitation polarization dependence and found the same $\cos^2$ variation as for the unshifted E_{11} emission, which is known to arise from transitions polarized parallel to the nanotube axis (Figure S6B).[20]

We performed a series of control experiments to understand the functionalization reaction. No spectral transformation occurred in samples that had been purged with argon to remove dissolved O_2 (see Figure S9). This shows the key role of oxygen. Irradiation of air-saturated ssDNA-suspended samples in the absence of rose bengal sensitizer similarly gave no transformations, suggesting the involvement of singlet oxygen. This was confirmed by a strongly enhanced transformation efficiency when the treatment was performed in D_2O (see Figure S10), a solvent known to extend the lifetime of $^1O_2$ by approximately an order of magnitude compared to H_2O.[21] The reaction also proceeded similarly when erythrosin B was substituted for rose bengal as a sensitizer, demonstrating that the dye is involved only as a generator of $^1O_2$ (see Figure S11, S12). Finally, treatment of SWCNTs suspended in conventional surfactants or in ssDNA oligos that lacked guanine nucleotides gave negligible spectral changes (see Figure S13). This result shows that the covalent functionalization reaction is specific to guanine.

The emission spectra of treated nanotubes depend on reaction parameters and SWCNT structure. For a given ssDNA oligo that contains guanine, the shift of the E_{11}^* peak position from

the pristine value grows monotonically with increasing dose of $^1O_2$, approaching an asymptotic value (see Figure 2A). Under our normal reaction conditions, $^1O_2$ dose is proportional to the initial concentration of sensitizer dye because the dye is fully degraded during irradiation. A plot of Raman D/G band intensity ratio (Figure 2F) confirms the smooth increase in sample functionalization with dye concentration. This trend is also seen in the progressive broadening and red-shifting of features in the sample's absorption spectrum (Figure 2E).

We also find that the asymptotic emission peak shift and width show a strong inverse dependence on nanotube diameter. Notably, the E_{11} shift decreases by more than a factor of five for nanotube diameter increases from 0.757 to 1.032 nm. Figure 2A,B plot these quantities vs the minimum radius of curvature for C-C bonds in each species. This minimum radius combines nanotube diameter with bond orientation to show the maximum bond strain. We propose that the functionalization process involves two steps (see Scheme 1 below). The first is reaction of $^1O_2$ (formed through rose bengal sensitization) with guanine nucleosides to form guanine endoperoxide. The second is reaction of the resulting peroxyradical with the adjacent nanotube surface. Our findings are consistent with a rate-limiting second step whose rate and yield are enhanced by curvature-induced bond strain in the nanotube. This would increase the fraction of reacted guanine sites in smaller diameter SWCNTs and lead to more pronounced spectral changes. Alternatively, it may be that the functionalization densities are similar throughout the sample but larger band gap species show greater spectral perturbations. However, measured spectral shifts show a much poorer correlation with E_{11} (Fig. S15) than with curvature (Fig. 2C), suggesting that bond strain is the dominant factor.

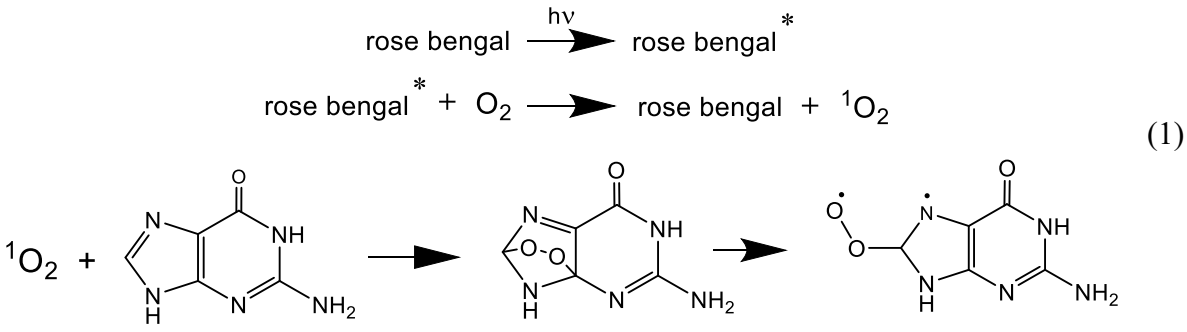

(1)

A significant finding is that the final spectral shifts are controlled by the guanine content of the ssDNA coating. Figure 3A illustrates this effect, where the red-shifts increase nearly proportionally to the fraction of G bases in the ssDNA oligo varies from 0 to 67%. We note that this smooth dependence on G content allows tuning of emission wavelengths by up to 10% for smaller diameter SWCNTs (see Table 1). For context, these shifts are smaller than the fixed shifts induced by covalent doping with oxygen atoms or aryl groups. The E_{11}^* width also increases with G content (see Figure 3B), although this increase is sub-linear and seems to saturate at high values. Our observation of spectral shifts controlled by the density of functionalization sites is quite different from the behavior of SWCNTs sparsely doped with oxygen atoms, in which higher functionalization density increases the intensity of the E_{11}^* emission without changing its wavelength.[2]

The guanine-controlled spectral shifts found here imply that the energy of a nanotube exciton is affected by multiple functionalization sites. This can occur if the spatial extent of the exciton is large enough to span several neighboring functionalization positions. It is known that SWCNT excitons are mobile,[22] so one might expect them to preferentially migrate to lower energy regions associated with high functionalization densities. To test this concept, we prepared SWCNT dispersions using “tandem” DNA oligos composed of two segments with different

guanine contents. An example is $(GT)_{30}(TGTT)_{15}$, in which the first segment contains 50% G and the second contains 25% G. It is informative to compare spectra from this tandem sample with those treated in pure $(GT)_{20}$ and in pure $(TGTT)_{10}$ (which are spectrally equivalently to $(GT)_{30}$ and $(TGTT)_{15}$). The absorption spectra in Figure 3D show that the tandem sample peak near 1160 nm falls rather near the average peak position of the pure reference samples. (The feature near 1280 nm is less relevant because of its much smaller shift with functionalization.) This observation is consistent with equal nanotube absorption within the separate segments. By contrast, emission spectra plotted in Figure 3C reveal that the E_{11}^* peaks in the tandem oligo coating lie much closer to those in $(GT)_{20}$ than to an average of the $(GT)_{20}$ and $(TGTT)_{10}$ positions. This shows that excitons are not delocalized over regions containing both segments, but instead become confined and emit within the $(GT)_{30}$ segment, where the optical band gap is lower by at least a few times k_BT. Additional experiments using mixtures of separate oligos confirmed these conclusions (see Figure S16 and S17).

To assess the number of adjacent functionalization sites influencing a localized exciton, we note the report of Salem *et al*.,[23] which concluded that ssDNA at higher ionic strengths forms a relatively compact helical structure on SWCNT surfaces. Estimating that helical pitch to be approximately 2 nm, and using a value of 0.676 nm for the average linear base spacing in ssDNA,[24] we obtain an axial separation between guanines of ~0.4 nm for $(GT)_n$. Theoretical and experimental studies predict the size of SWCNT excitons, described by average electron-hole separations, to be at least five times this value,[25-28] so it seems reasonable that excitons trapped in treated nanotubes feel the cumulative potential of several nearby guanine functionalization sites. This can explain how the E_{11}^* spectral shifts are controlled by the spatial density of guanine nucleotides in the oligo base sequence.

We performed further experiments to probe the effects of ssDNA oligo length, nucleotide sequence, and guanine content on SWCNT modification. Samples of SWCNTs in $(GT)_{10}$, $(GT)_{20}$, and $(GT)_{30}$ were treated under the same conditions. The samples in $(GT)_{20}$ and $(GT)_{30}$ showed similar SWCNT spectral changes, whereas SWCNTs in the short $(GT)_{10}$ oligos were slightly less spectrally perturbed (Figure S19). We deduce that SWCNT functionalization is insensitive to ssDNA length except for the shortest oligos, which may not be optimally wrapped on the SWCNTs.[29]

We foresee interesting uses for guanine-functionalized nanotubes. In biological media, the covalent links between ssDNA and SWCNT confer high stability, preventing displacement of the DNA coating even by high concentrations of proteins. To demonstrate this, we incubated samples of pristine and treated SWCNTs for 17 h in a solution with 150 mg/dL of fibrinogen, simulating physiological conditions.[30] The treated SWCNTs remained suspended whereas the pristine sample showed strong aggregation. As displayed in Figure 4A, fluorescence spectra of the two supernatants extracted after mild centrifugation are dramatically different, with no measurable emission remaining from the untreated sample exposed to fibrinogen. Exposure for 20 h to another plasma protein, 5% BSA,[31] caused no change in emission from a treated SWCNT sample (see Figure S21). These results show the stability of guanine-functionalized SWCNTs and suggest the potential for biomedical applications. For example, it will be possible to disperse SWCNTs in ssDNA oligos that contain guanines only near their ends and covalently anchor them using the singlet oxygen reaction. The unreacted DNA segments may then be used for covalent linkage reactions to antibodies, peptides, or therapeutic agents in applications requiring a robust near-IR emissive tag.

Another area of potential application involves using oligos with specific base sequences as spatial templates to modulate nanotube electronic structure. This concept is illustrated in Figure 4B, which represents a SWCNT wrapped by a tandem ssDNA oligo in which one segment contains 50% guanines and the other only 25% guanines. After treatment to induce covalent functionalization at the guanine sites, the higher density of those sites in the guanine-rich segment gives a region of lowered energy for electrons and excitons as compared to the neighboring region. The spectra in Figure 3C show the resulting exciton migration to the more heavily functionalized regions. In unexcited nanotubes, we expect adjacent regions to display *p*-doped and *n*-doped character, forming *p*-*n* junctions within individual nanotubes. The ability to engineer spatially modulated electronic structures through choice of ssDNA sequence may enable innovative electro-optic applications based on custom functionalized nanotubes. For example, one can create quantum defects with controllable trap depth and spacing for potential single-photon emission applications in quantum cryptography.

CONCLUSIONS

In conclusion, we have found that exposure of ssDNA-coated SWCNTs to singlet oxygen gives covalent functionalization of guanine nucleobases to the nanotube sidewall. The resulting covalent hybrids show near-infrared fluorescence that is red-shifted, broadened, and intensified compared to pristine SWCNTs. The degree of spectral shift and broadening is directly related to the spatial density of guanines in the ssDNA oligo and can therefore be selected by choice of ssDNA structure. No reduction in fluorescence intensity was observed even at the highest functionalization densities. The use of tandem ssDNA oligos containing regions of differing guanine contents allows control of the spatial pattern as well as the modulation depth of excitonic energies within individual functionalized SWCNTs. We expect that other methods for

spatial patterning of nanotube electronic structure may also emerge from further studies of chemical reactions with structured coatings.

MATERIALS AND METHODS

Preparation of SWCNT samples. Custom-synthesized ssDNA (Sigma-Aldrich) solutions contained 0.1 M sodium chloride and 0.06 M sodium phosphate buffer (pH = 7.4). HiPco SWCNTs were grown in the Rice University reactor (Batch ID 195.1) and CoMoCAT material (type SG65) was purchased from SouthWest NanoTechnologies, Inc. Raw SWCNTs were added to the ssDNA solution in a weight ratio of 1:2. The mixture was kept in an ice-water bath and dispersed using tip sonication at 4 W output power (3 mm tip, Misonix Microson XL) for 30 active minutes (60 min with duty cycle of 30 s on, 30 s off). The suspension was then centrifuged for 2 h at 13,000 g in a Biofuge-13 (Baxter Scientific). Finally, we collected the supernatant and diluted it with 0.1 M NaCl and 0.06 M NaH_2PO_4/Na_2HPO_4 buffer (pH = 7.4) for characterization. A stock solution of rose bengal was prepared at a fixed concentration of 330 μM. Aqueous solutions of 1% and 5% (w/v) sodium deoxycholate (SDC) were prepared for use in coating displacement. Type I fibrinogen from human plasma was purchased from Sigma-Aldrich.

Functionalization of suspended SWCNTs. The rose bengal stock solution of was added to 500 μL SWCNT samples, and the mixtures were then irradiated at 532 nm (laser power of ca. 260 mW). The added volume of rose bengal stock solution was varied to investigate the extent of SWCNT functionalization.

Absorption spectroscopy. Absorption spectra were measured using a prototype model NS2 NanoSpectralyzer (Applied NanoFluorescence, LLC). The optical path length was 1 cm.

Short-wave infrared (SWIR) fluorescence spectroscopy. SWIR spectra were measured with the prototype model NS2 NanoSpectralyzer using fixed excitation wavelengths of 642nm, 659 nm, and 784 nm. Two-dimensional excitation-emission maps were measured using a custom apparatus in which a SuperK EXTREME supercontinuum white light laser source (NKT Photonics) followed by a SuperK Varia (NKT Photonics) filter provided tunable excitation. This beam was passed through a KG5 filter (Schott) to block stray SWIR emission. For all maps, the sample was excited with a 10 nm bandwidth, covering wavelengths from 524 to 800 nm with a step size of 2 nm. The excitation beam irradiated the sample, held in a 1 cm path length cuvette, without focusing. SWIR emission was collected at a 90° angle from excitation directly into the 105 μm core of an optical fiber placed close to the sample. The emission was transmitted to a spectrometer (B&WTek Sol 1.7) with a 512-channel InGaAs array cooled to -15 °C. We used a 1 s integration time to acquire each emission spectrum. The instrument and data acquisition were computer-controlled by custom LabVIEW software.

Raman spectroscopy. A prototype model NS3 NanoSpectralyzer (Applied NanoFluorescence, LLC) was used to obtain Raman spectra with 671 nm laser excitation.

SWIR fluorescence microscopy and imaging. Spectra and images of individual SWCNTs were measured using a customized SWIR fluorescence microscopy system described elsewhere.[20] SWCNT samples were first heavily diluted using 1% SDC. Next, these samples were drop-cast onto plastic cover slips, dried, placed onto a glass microscope slide, and mounted onto the microscope stage. The immobilized SWCNTs were excited using a tunable CW Ti:Sapphire laser. The linear polarization state of this laser was controlled using a Glan-Thompson calcite polarizer and a $\lambda/2$ retardation plate. SWIR emission was collected using a Nikon PlanApo 60x /1.27 NA water immersion objective and passed through a 950 nm long-pass

filter and a dichroic beam splitter to reject stray excitation light and short wavelength emission. Emission images were taken by a Roper Scientific OMA-V 2D InGaAs camera at an integration time of 200 ms. Emission spectra were collected by directing the microscope's image plane to an optical fiber (ThorLabs, 105 μm core diameter) leading to the input slit of a spectrograph (J-Y C140) coupled to a 512 pixel linear InGaAs array detector (Roper Scientific OMA-V). Spectra were acquired with a 50 s integration time.

ASSOCIATED CONTENT

An earlier version of this report was submitted to a pre-print server.[32]

Supporting Information

The Supporting Information is available free of charge on the ACS Publications website.

Figures showing additional absorption, fluorescence, and excitation-emission spectra for bulk samples; emission spectra and images of individual nanotubes; further results relating to mixed SWCNT coatings and effects of ssDNA length and added NaCl. Supplementary tables of spectral parameters.

Financial Interest Statement

The authors declare the following competing financial interest: R. B. W. has a financial interest in Applied NanoFluorescence, LLC, which manufactures some of the instruments used in this project.

AUTHOR INFORMATION

Corresponding Author

weisman@rice.edu. Tel: 713-3483709. Fax: 713-348-5155.

ORCID

Yu Zheng: 0000-0003-2703-9143

Sergei M. Bachilo: 0000-0001-5236-1383

R. Bruce Weisman: 0000-0001-8546-9980

ACKNOWLEDGEMENTS

This research was supported by grants from the National Science Foundation (CHE-1803066) and the Welch Foundation (C-0807).

REFERENCES

1. Reich, S.; Thomsen, C.; Maultzsch, J., *Carbon Nanotubes: Basic Concepts and Physical Properties*. John Wiley & Sons: Hoboken, 2008.
2. Ghosh, S.; Bachilo, S. M.; Simonette, R. A.; Beckingham, K. M.; Weisman, R. B. Oxygen Doping Modifies near-Infrared Band Gaps in Fluorescent Single-Walled Carbon Nanotubes. *Science* **2010,** *330*, 1656-1659.
3. Piao, Y.; Meany, B.; Powell, L. R.; Valley, N.; Kwon, H.; Schatz, G. C.; Wang, Y. Brightening of Carbon Nanotube Photoluminescence through the Incorporation of sp^3 Defects. *Nature Chem.* **2013,** *5*, 840-845.
4. Wu, X.; Kim, M.; Kwon, H.; Wang, Y. Photochemical Creation of Fluorescent Quantum Defects in Semiconducting Carbon Nanotube Hosts. *Angew. Chem.* **2018,** *130*, 656-661.
5. Kwon, H.; Furmanchuk, A. o.; Kim, M.; Meany, B.; Guo, Y.; Schatz, G. C.; Wang, Y. Molecularly Tunable Fluorescent Quantum Defects. *J. Am. Chem. Soc.* **2016,** *138*, 6878-6885.
6. Shiraki, T.; Shiraishi, T.; Juhász, G.; Nakashima, N. Emergence of New Red-Shifted Carbon Nanotube Photoluminescence Based on Proximal Doped-Site Design. *Sci. Rep.* **2016,** *6*, 28393.
7. Kim, M.; Adamska, L.; Hartmann, N. F.; Kwon, H.; Liu, J.; Velizhanin, K. A.; Piao, Y.; Powell, L. R.; Meany, B.; Doorn, S. K.; Tretiak, S.; Wang, Y. Fluorescent Carbon Nanotube Defects Manifest Substantial Vibrational Reorganization. *J. Phys. Chem. C* **2016,** *120*, 11268-11276.
8. He, X.; Hartmann, N. F.; Ma, X.; Kim, Y.; Ihly, R.; Blackburn, J. L.; Gao, W.; Kono, J.; Yomogida, Y.; Hirano, A.; Tanaka, T.; Kataura, H.; Htoon, H.; Doorn, S. K. Tunable Room-Temperature Single-Photon Emission at Telecom Wavelengths from sp^3 Defects in Carbon Nanotubes. *Nat. Photonics* **2017,** *11*, 577-582.
9. Ma, X.; Hartmann, N. F.; Baldwin, J. K. S.; Doorn, S. K.; Htoon, H. Room-Temperature Single-Photon Generation from Solitary Dopants of Carbon Nanotubes. *Nat. Nanotechnol.* **2015,** *10*, 671-675.
10. Saha, A.; Gifford, B. J.; He, X.; Ao, G.; Zheng, M.; Kataura, H.; Htoon, H.; Kilina, S.; Tretiak, S.; Doorn, S. K. Narrow-Band Single-Photon Emission through Selective Aryl Functionalization of Zigzag Carbon Nanotubes. *Nature Chem.* **2018,** *10*, 1089-1095.
11. Zheng, M.; Jagota, A.; Semke, E. D.; Diner, B. A.; McLean, R. S.; Lustig, S. R.; Richardson, R. E.; Tassi, N. G. DNA-Assisted Dispersion and Separation of Carbon Nanotubes. *Nat. Mater.* **2003,** *2*, 338-342.
12. Zheng, M.; Jagota, A.; Strano, M. S.; Santos, A. P.; Barone, P.; Chou, S. G.; Diner, B. A.; Dresselhaus, M. S.; McLean, R. S.; Onoa, G. B.; Samsonidze, G. G.; Semke, E. D.; Usrey, M.; Watts, D. J. Structure-Based Carbon Nanotube Sorting by Sequence-Dependent DNA Assembly. *Science* **2003,** *302*, 1545-1548.
13. Ludvíková, L.; Friš, P.; Heger, D.; Šebej, P.; Wirz, J.; Klán, P. Photochemistry of Rose Bengal in Water and Acetonitrile: A Comprehensive Kinetic Analysis. *Phys. Chem. Chem. Phys.* **2016,** *18*, 16266-16273.
14. Kawanishi, S.; Inoue, S.; Sano, S.; Aiba, H. Photodynamic Guanine Modification by Hematoporphyrin is Specific for Single-Stranded DNA with Singlet Oxygen as a Mediator. *J. Biol. Chem.* **1986,** *261*, 6090-6095.
15. Ravanat, J.-L.; Martinez, G. R.; Medeiros, M. H. G.; Di Mascio, P.; Cadet, J. Mechanistic Aspects of the Oxidation of DNA Constituents Mediated by Singlet Molecular Oxygen. *Arch. Biochem. Biophys.* **2004,** *423*, 23-30.

16. Cadet, J.; Ravanat, J. L.; Martinez, G. R.; Medeiros, M. H. G.; Di Mascio, P. Singlet Oxygen Oxidation of Isolated and Cellular DNA: Product Formation and Mechanistic Insights. *Photochem. Photobiol.* **2006,** *82*, 1219-1225.

17. Agnez-Lima, L. F.; Melo, J. T. A.; Silva, A. E.; Oliveira, A. H. S.; Timoteo, A. R. S.; Lima-Bessa, K. M.; Martinez, G. R.; Medeiros, M. H. G.; Di Mascio, P.; Galhardo, R. S.; Menck, C. F. M. DNA Damage by Singlet Oxygen and Cellular Protective Mechanisms. *Mutat. Res., Rev. Mutat. Res.* **2012,** *751*, 15-28.

18. Graupner, R. Raman Spectroscopy of Covalently Functionalized Single-Wall Carbon Nanotubes. *J. Raman Spectrosc.* **2007,** *38*, 673-683.

19. Zheng, Y.; Bachilo, S. M.; Weisman, R. B. Enantiomers of Single-Wall Carbon Nanotubes Show Distinct Coating Displacement Kinetics. *J. Phys. Chem. Lett.* **2018,** *9*, 3793-3797.

20. Tsyboulski, D. A.; Bachilo, S. M.; Weisman, R. B. Versatile Visualization of Individual Single-Walled Carbon Nanotubes with near-Infrared Fluorescence Microscopy. *Nano Lett.* **2005,** *5*, 975-979.

21. Lindig, B. A.; Rodgers, M. A. J.; Schaaplc, A. P. Determination of the Lifetime of Singlet Oxygen in D_2O Using 9,10-Anthracenedipropionic Acid, a Water-Soluble Probe. *J. Am. Chem. Soc.* **1980,** *102*, 5590-5593.

22. Cognet, L.; Tsyboulski, D.; Rocha, J.-D. R.; Doyle, C. D.; Tour, J. M.; Weisman, R. B. Stepwise Quenching of Exciton Fluorescence in Carbon Nanotubes by Single-Molecule Reactions. *Science* **2007,** *316*, 1465-1468.

23. Salem, D. P.; Gong, X.; Liu, A. T.; Koman, V. B.; Dong, J.; Strano, M. S. Ionic Strength-Mediated Phase Transitions of Surface-Adsorbed DNA on Single-Walled Carbon Nanotubes. *J. Am. Chem. Soc.* **2017,** *139*, 16791-16802.

24. Chi, Q.; Wang, G.; Jiang, J. The Persistence Length and Length Per Base of Single-Stranded DNA Obtained from Fluorescence Correlation Spectroscopy Measurements Using Mean Field Theory. *Phys. A (Amsterdam, Neth.)* **2013,** *392*, 1072-1079.

25. Perebeinos, V.; Tersoff, J.; Avouris, P. Scaling of Excitons in Carbon Nanotubes. *Phys. Rev. Lett.* **2004,** *92*, 257402.

26. Capaz, R. B.; Spataru, C. D.; Ismail-Beigi, S.; Louie, S. G. Diameter and Chirality Dependence of Exciton Properties in Carbon Nanotubes. *Phys. Rev. B* **2006,** *74*, 121401.

27. Kilina, S.; Tretiak, S. Excitonic and Vibrational Properties of Single-Walled Semiconducting Carbon Nanotubes. *Adv. Funct. Mater.* **2007,** *17*, 3405-3420.

28. Mann, C.; Hertel, T. 13 Nm Exciton Size in (6,5) Single-Wall Carbon Nanotubes. *J. Phys. Chem. Lett.* **2016,** *7*, 2276-2280.

29. Zheng, Y.; Bachilo, S. M.; Weisman, R. B. Quenching of Single-Walled Carbon Nanotube Fluorescence by Dissolved Oxygen Reveals Selective Single-Stranded DNA Affinities. *J. Phys. Chem. Lett.* **2017,** *8*, 1952-1955.

30. Chen, R.; Radic, S.; Choudhary, P.; Ledwell, K. G.; Huang, G.; Brown, J. M.; Ke, P. C. Formation and Cell Translocation of Carbon Nanotube-Fibrinogen Protein Corona. *Appl. Phys. Lett.* **2012,** *101*.

31. Carter, D. C.; Ho, J. X. Structure of Serum Albumin. In *Advances in Protein Chemistry*; Anfinsen, C. B.; Edsall, J. T.; Richards, R. M.; Eisenberg, D. S., Eds.; Academic Press: New York, 1994; pp 153-176.

32. Zheng, Y.; Bachilo, S. M.; Weisman, R. B. Controlled Patterning of Carbon Nanotube Energy Levels by Covalent DNA Functionalization. 2019, 7881221.v1. ChemRxiv. https://doi.org/10.26434/chemrxiv.7881221.v1 (accessed 3/25/2019).

Table 1. Dependence of spectral emission parameters of treated SWCNT species on ssDNA coating guanine content. % G shows the percentage of guanine bases present in the ss-DNA oligo.

% G	ssDNA sequence	E_{11}* peak position (nm)				E_{11}* peak width (meV)			
		(6,5)	(7,5)	(7,6)	(9,5)	(6,5)	(7,5)	(7,6)	(9,5)
50	$(GT)_{20}$ untreated	992	1041	1143	1266	30	28	25	31
0	T_{30}	992	1042	1143	1268	31	30	25	29
16.7	$(TGT)_{10}(TCC)_{10}$	1018	1060	1158	1282	73	62	56	39
25	$(TGTT)_{10}$	1023	1069	1160	1284	74	69	58	42
33.3	$(TGT)_{15}$	1050	1075	1177	1286	99	72	63	45
37.5	$(GT)_{30}(TGTT)_{15}$	1064	1095	1195	1291	101	83	78	54
38.3	$(GT)_{16}(TGTT)_{7}$	1056	1085	1185	1288	100	81	75	48
41.7	$(GT)_{15}(TGT)_{10}$	1059	1081	1183	1288	100	79	74	47
50	$(GA)_{20}$	1042	1070	1173	1286	101	71	65	45
50	$(GC)_{20}$	1072	1103	1200	1291	103	86	78	55
50	$(GT)_{20}$	1070	1105	1209	1296	103	89	82	56
66.7	$(GTG)_{15}$	1098	1126	1225	1305	105	91	82	56
	O-doped [a]	1120	1155	1266		50	56	80	
	Aryl-doped [b]	1137	1179	1263		57	70	59	

[a] Ghosh *et al*.[2]
[b] Piao *et al*.[3]

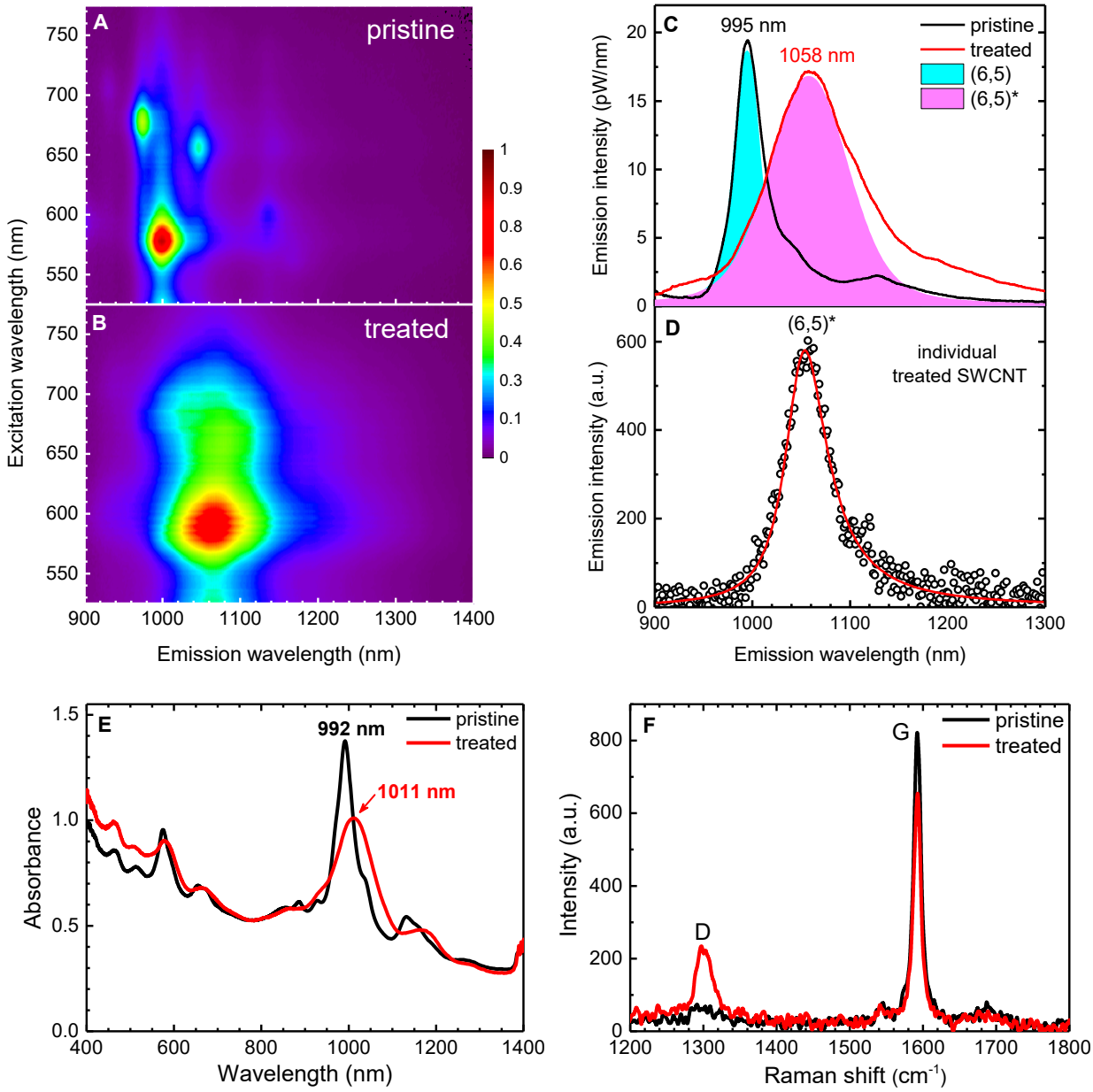

Figure 1. Photoluminescence excitation-emission contour plots for CoMoCAT SWCNTs dispersed in a $(GT)_{20}$ solution **(A)** before and **(B)** after exposure to $^1O_2$. **(C)** Fluorescence spectra at (6,5) excitation wavelength before and after treatment. **(D)** Fluorescence spectrum of an individual treated (6,5)* after coating displacement by 1% SDC. **(E)** Absorption and **(F)** Raman spectra before and after treatment.

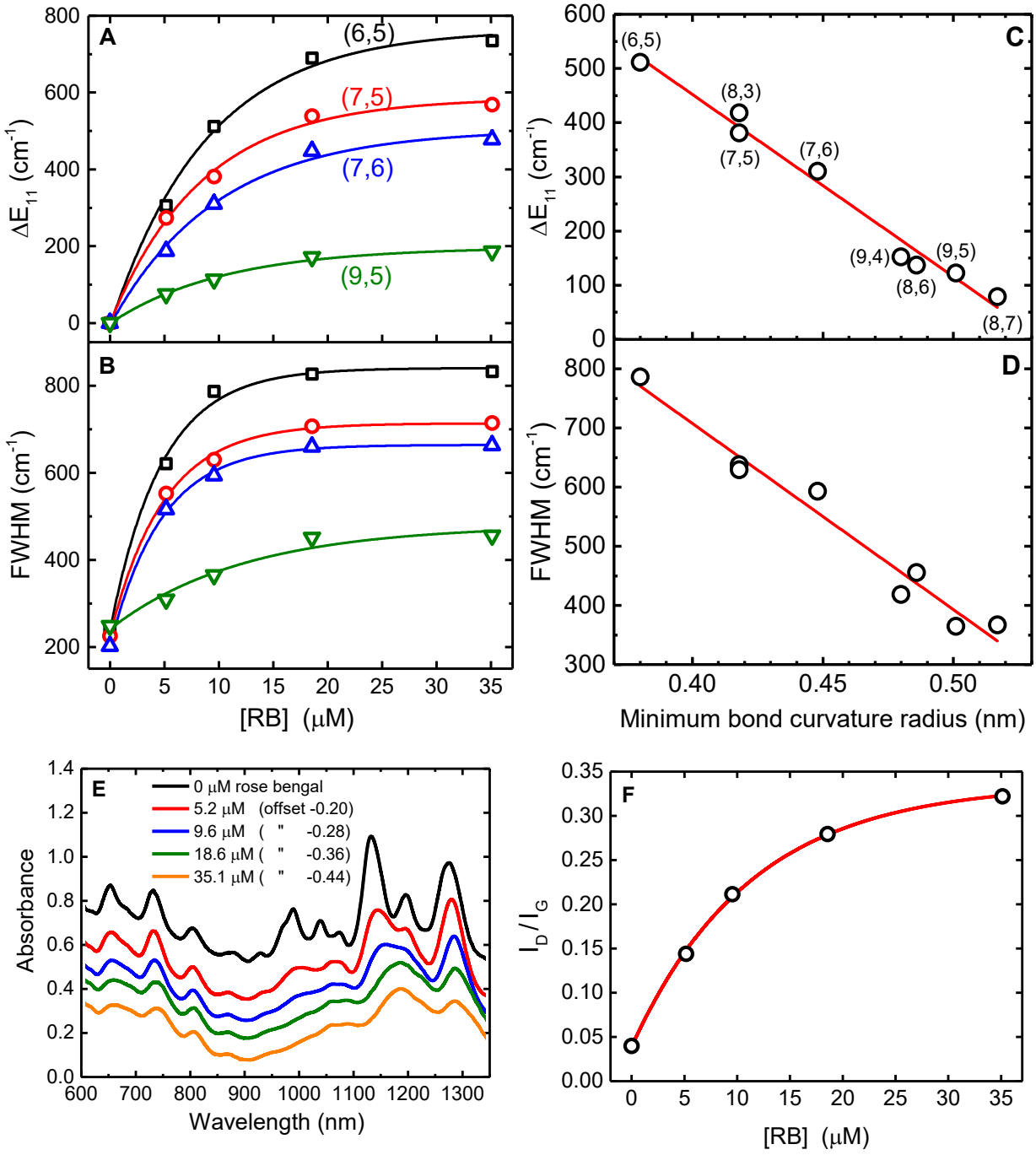

Figure 2. (A) E_{11} emission peak position shift and **(B)** treated E_{11} peak width vs. rose bengal concentration. **(C)** E_{11}^{*} peak position shift and **(D)** E_{11}^{*} peak width vs. radius of curvature of the most strained nanotube bond, for samples treated with 10 μM rose bengal sensitizer. **(E)** Absorption spectra of a HiPco sample following treatment in the presence of different concentrations of rose bengal sensitizer. **(F)** Raman D/G intensity ratio vs. initial concentration of rose bengal sensitizer.

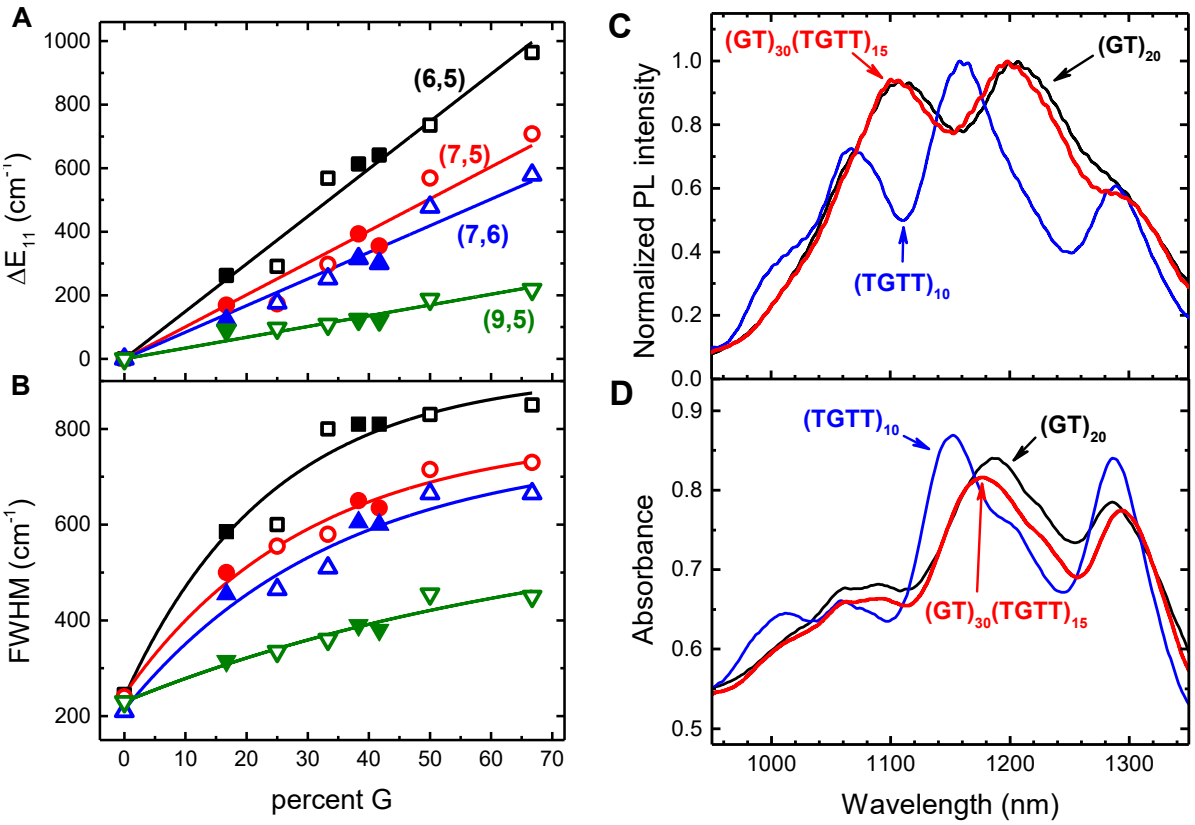

Figure 3. Asymptotic changes in SWCNT emission peak position **(A)** and width **(B)** induced by $^1O_2$ treatment vs. G content of the ssDNA coating. Filled symbols show data points measured with tandem ssDNA oligos. **(C)** Normalized asymptotic fluorescence spectra of $^1O_2$ -treated SWCNTs in $(GT)_{20}$ (black curve), $(GT)_{30}(TGTT)_{15}$ (red curve) and $(TGTT)_{10}$ (blue curve). **(D)** Absorption spectra of the samples from **(C)**, plus the average spectrum (green curve) of samples in $(GT)_{20}$ and $(TGTT)_{10}$.

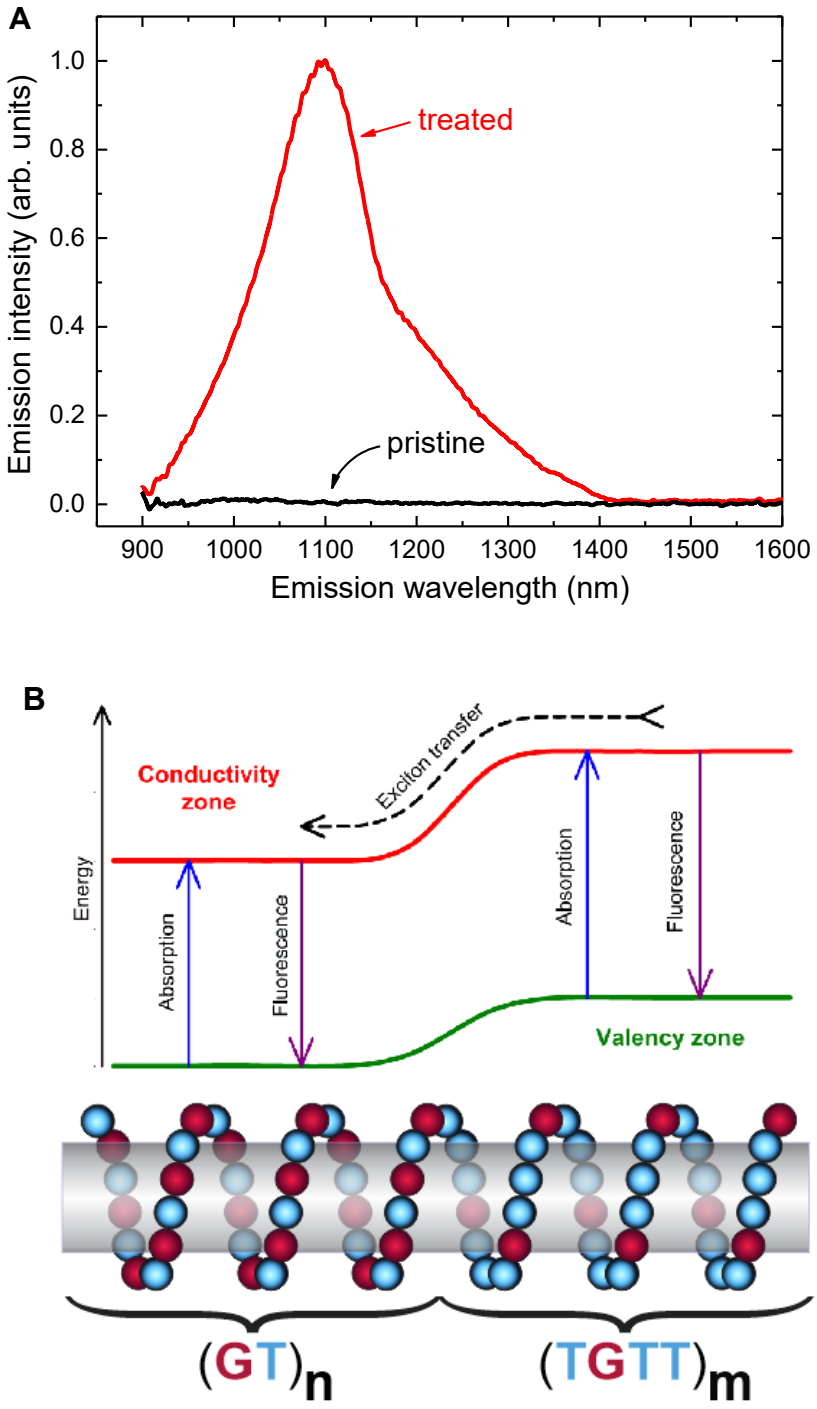

Figure 4. (A) Emission spectra of $^{1}O_2$ treated (red curve) and pristine (black curve) $(GT)_{20}$-SWCNT dispersions after exposure to physiological concentration of fibrinogen followed by centrifugation. (B) Conceptual sketch showing how exciton motion can be controlled in a SWCNT that is suspended in a tandem ssDNA oligo containing different guanine contents and then treated to induce functionalization.

For Table of Contents Only: